Water Research 224 (2022) 119094

Contents lists available at ScienceDirect

Water Research

journal homepage: www.elsevier.com/locate/watres

Inhibition of biofouling on reverse osmosis membrane surfaces by germicidal ultraviolet light side-emitting optical fibers

Hojung Rho [a,b,*], Pingfeng Yu [c,d], Zhe Zhao [a], Chung-Seop Lee [a], Kangmin Chon [e], François Perreault [a], Pedro J.J. Alvarez [c], Gary Amy [f], Paul Westerhoff [a]

[a] Nanosystems Engineering Research Center for Nanotechnology-Enabled Water Treatment, School of Sustainable Engineering and the Built Environment, Arizona State University, Tempe, Arizona 85287, USA
[b] Department of Environment Research, Korea Institute of Civil Engineering and Building Technology, 283 Goyang-Daero, Ilsanseo-Gu, Goyang-Si, Gyeonggi-Do 10223, Republic of Korea
[c] Nanosystems Engineering Research Center for Nanotechnology-Enabled Water Treatment, Department of Civil and Environmental Engineering, Rice University, Houston, Texas 77251, USA
[d] College of Environmental and Resource Sciences, Zhejiang University, Hangzhou 310058, China
[e] Department of Environmental Engineering, College of Art, Culture, and Engineering, Kangwon National University, 1 Kangwondaehak-gil, Chuncheon-si, Gangwon-do 24341, Republic of Korea
[f] College of Engineering and Science, Clemson University, Clemson, SC 29634, USA

ARTICLE INFO

Keywords:
Side-emitting optical fibers
Ultraviolet
disinfection
Biofouling
Reverse osmosis

ABSTRACT

Biofouling of membrane surfaces poses significant operational challenges and costs for desalination and wastewater reuse applications. Ultraviolet (UV) light can control biofilms while reducing chemical usage and disinfection by-products, but light deliveries to membrane surfaces in spiral wound geometries has been a daunting challenge. Thin and flexible nano-enabled side-emitting optical fibers (SEOFs) are novel light delivery devices that enable disinfection or photocatalytic oxidation by radiating UV light from light-emitting diodes (LEDs). We envision SEOFs as an active membrane spacer to mitigate biofilm formation on reverse osmosis (RO) membranes. A lab-scale RO membrane apparatus equipped with SEOFs allowed comparison of UV-A (photocatalysis-enabled) versus UV-C (direct photolysis disinfection). Compared against systems without any light exposure, systems with UV-C light formed thinner—but denser—biofilms, prevented permeate flux declines due to biofouling, and maintained the highest salt rejection. Results were corroborated by *in-situ* optical coherence tomography and *ex-situ* measurements of biofilm growth on the membranes. Transcriptomic analysis showed that UV-C SEOFs down-regulated quorum sensing and surface attachment genes. In contrast, UV-A SEOFs upregulated quorum sensing, surface attachment, and oxidative stress genes, resulting in higher extracellular polymeric substances (EPS) accumulation on membrane surfaces. Overall, SEOFs that deliver a low fluence of UV-C light onto membrane surfaces are a promising non-chemical approach for mitigating biofouling formation on RO membranes.

1. Introduction

Reverse osmosis (RO) desalination of seawater, brackish ground water, municipal wastewater effluents, industrial wastewater, and other water sources is central to increasing the water supply for high-quality water (Park et al., 2016; Shannon et al., 2009). A major challenge for RO technology is the decline in performance (*i.e.,* permeate water flux and solute rejection) and increase in energy requirements due to fouling by organic matter, inorganic scalants, and/or bacterial biofilms on the membrane surface (Jafari et al., 2021; Mo et al., 2012; Rana and Matsuura, 2010). Biofouling is a major contributor to increases in RO membrane operational cost because it increases pressure requirements, decreases water fluxes, and increases chemical use (Bar-Zeev et al., 2015a; Mansouri et al., 2010; Matin et al., 2011). Numerous strategies have been explored to mitigate biofilm formations, including pretreatment to remove biodegradable organic matter, adding chemicals to

* Corresponding author at: Nanosystems Engineering Research Center for Nanotechnology-Enabled Water Treatment, School of Sustainable Engineering and the Built Environment, Arizona State University, Tempe, Arizona 85287, USA.
E-mail address: hojungrho@kict.re.kr (H. Rho).

https://doi.org/10.1016/j.watres.2022.119094
Received 19 June 2022; Received in revised form 28 August 2022; Accepted 8 September 2022
Available online 10 September 2022

disinfect biofilms, or modifying membrane materials for antifouling; however, their use alone or in combination has yet to eliminate biofilm formation on RO membranes. To avoid the formation of by-products (*e.g.,* nitrosamines) associated with adding chemical disinfectants (*e.g.,* chloramines) during RO treatment, non-chemical strategies are needed to mitigate biofouling and reduce the operational costs associated with RO treatment (Bar-Zeev et al., 2015b).

Biofilms are surface-bound complex microbial aggregates encased in self-produced extracellular polymeric substances (EPS) that are primarily composed of polysaccharides and proteins (Herzberg and Elimelech, 2007; Herzberg et al., 2009; Rosenberg and DeLong, 2013). Because of protection provided by the EPS matrix, once established, biofilms have a strong resistance to chemical penetration and hydraulic cleaning cycles (Flemming and Wingender, 2010). Bacteria reportedly produce more EPS under stress conditions, thus requiring excessive cleaning agents to control biofouling in RO membrane processes, which leads to secondary environmental pollution and periodic shut-down of the processes (Freire-Gormaly and Bilton, 2019; Soule et al., 2016). Additionally, polyamide membranes inevitably degrade during chlorine-based cleaning cycles and require more frequent replacement. Therefore, there is a need to understand how new biofouling control technologies influence biological processes and/or the degradation of membrane materials.

Germicidal ultraviolet (UV) light is a proven viable non-chemical disinfection strategy for water treatment (Beck et al., 2016; Dotson et al., 2012; Linden et al., 2019). Traditionally, ultraviolet (UV) lamps use low-pressure (LP) monochromatic UV light or medium-pressure (MP) polychromatic UV light generated from mercury sources (Bolton and Cotton, 2011). Ultraviolet light-emitting diodes (UV-LED) are emerging for specialty disinfection applications because they are mercury-free and compact, require low power, and have long life expectancy (Linden et al., 2019; Muramoto et al., 2014; Sholtes et al., 2016). LED wavelengths can be selected to disinfect bacteria through different mechanisms (Beck et al., 2018; Beck et al., 2017; Sholtes et al., 2016) or be used to initiate photocatalysis in the presence of titanium dioxide (TiO_2) or other photocatalysts (Chen et al., 2017; Ling et al., 2017; Loeb et al., 2019). A challenge for UV-LEDs is their relatively low power and ability to deliver light in different reactor configurations. Delivering light is particularly challenging for spiral-wound RO membranes that have water flowing through narrow channels.

Flexible plastic spacers are used in RO systems to maintain the channels and induce surface turbulence, which helps mitigates membrane fouling. A potential strategy to deliver UV light to membrane surfaces could involve replacing or integrating the flexible spacers with small-diameter (250–1000 μm), flexible side-emitting optical fibers (SEOFs) coupled with UV-LEDs. SEOFs have been developed to deliver light to surfaces or create high-surface-area photocatalysis processes (Lanzarini-Lopes et al., 2019; Lanzarini-Lopes et al., 2020; O'Neal Tugaoen et al., 2018; Song et al., 2021). UV-A wavelengths delivered into optical fibers (OFs) coated with TiO_2 nanoparticles effectively generate reactive oxygen species (ROS) (Ling et al., 2017; Song et al., 2021), which can degrade organic matter and contribute to microbial inactivation. UV-B and UV-C wavelengths are more effective for disinfection than UV-A because of the action spectra of DNA and proteins in bacteria (Beck et al., 2016; Beck et al., 2017). While modest levels of UV irradiation slightly oxidizes RO membranes to increase water flux while maintaining high salt rejections, it is important to acknowledge that excessive amounts of ROS and UV irradiation can degrade polymeric membrane materials (Nasrollahi et al., 2021; Rho et al., 2021). Therefore, we envision that SEOFs can replace or be integrated with inert plastic membrane spacers that are used in all spiral-wound RO membrane modules to deliver low UV fluence levels sufficient to inactivate bacteria or produce ROS for disinfection plus oxidation of soluble microbial products that accumulate on the membrane.

Although a few studies have reported using UV irradiation on a membrane module to reduce fouling in membrane processes (Molinari et al., 2019; Mozia, 2010; Song et al., 2012; Wei et al., 2019), these have all relied on irradiating flat sheet membranes by a point-source of light, including single or multiple LEDs placed at a distance from the membrane surface. However, such designs are not scalable to the spiral-wound modules that dominate most full-scale RO membrane processes. As such, we designed a RO membrane apparatus equipped with SEOFs to investigate and compare how UV-A (photocatalysis-enabled) versus UV-C (direct photolysis disinfection) influenced RO surface biofouling and associated membrane performance (*i.e.,* water flux and salt rejection). The design integrated SEOFs in a cross-flow membrane apparatus, allowing *in-situ* monitoring by optical coherence tomography (OCT) of biofilm density over time and at the end of the experiment, *ex-situ* monitoring and analysis of biofilm composition (EPS, proteins), and transcriptomic analysis of gene expression in response to UV light.

First, we characterized the side-emission of light and photocatalytic capabilities of the UV-C versus UV-A SEOFs. Second, we measured and compared the water flux, salt rejection, and biofilm surface density for membranes without light versus membranes enabled by UV-C versus UV-A SEOFs. Third, we quantified the changes in membrane properties after exposure to UV-C or UV-A light by SEOFs. Finally, we used cell counts, chemical analysis of membrane foulants, and transcriptomic analysis of the biofilms to discuss potential mechanisms for how the two different wavelength SEOFs influenced biofilm mitigation on RO membrane surfaces. This study provides valuable insights into novel biofouling-mitigation strategies for membrane-based processes, which will ultimately enhance the sustainability of desalination and water reuse efforts.

2. Materials and methods

2.1. SEOF-enabled RO membrane apparatus

Fig. 1 shows a custom RO membrane apparatus equipped with two SEOFs. Fig. 1a shows a fully-enclosed membrane cell that allows water cross-flow through the chamber, which is equipped with a quartz window to enable *in-situ* OCT measurements of biofilm density on the membrane surface. The photograph in Fig. 1b shows two SEOFs that are "glowing" (i.e., side-emitting light) when connected to a functioning LED, which is located outside the membrane cell. SEOFs are positioned less than 1 mm from the RO membrane surface. Fig. 1c shows the membrane cell configured within a temperature-controlled recirculating system. While the current experiment utilizes flat-sheet membranes, Fig. 1d shows one concept that could be explored to integrate flexible SEOFs as spacers within spiral-wound RO membrane modules.

The membrane cell included three primary components. First, membrane coupons with dimensions of 50 cm^2 were cut from a commercial brackish water reverse osmosis (BWRO) membrane element (MPD-based thin-film composite PA; Applied Membrane Inc., M-T1812A24). Prior to all experiments, the chemical coatings on the active layer of the RO membrane coupons were completely removed by soaking overnight in deionized (DI) water. Second, SEOFs were fabricated (see below) and placed within a 1 mm thick spacer (Fig. 1b) and connected, outside the cell, to different LEDs. Third, UV-LEDs (UV-C: 60 mW, Crystal IS, NY; UV-A: 1 W, NVSU233B, Nichia Corporation, Japan) at 265 nm and 365 nm were used for UV-C and UV-A SEOFs, respectively. The same electric current (0.45 amp) was applied to LEDs with different wavelengths. During all experiments, separate parallel membrane cells were operated using a common feed tank such that both the control (*i.e.*, SEOF without LED illumination) and treated (*i.e.*, SEOF with LED illumination) received the same bacterial concentrations over the 8-day experiment.

2.2. Performance test of RO membrane equipped with UV-SEOFs

The biofouling propensity and salt rejection of RO membrane

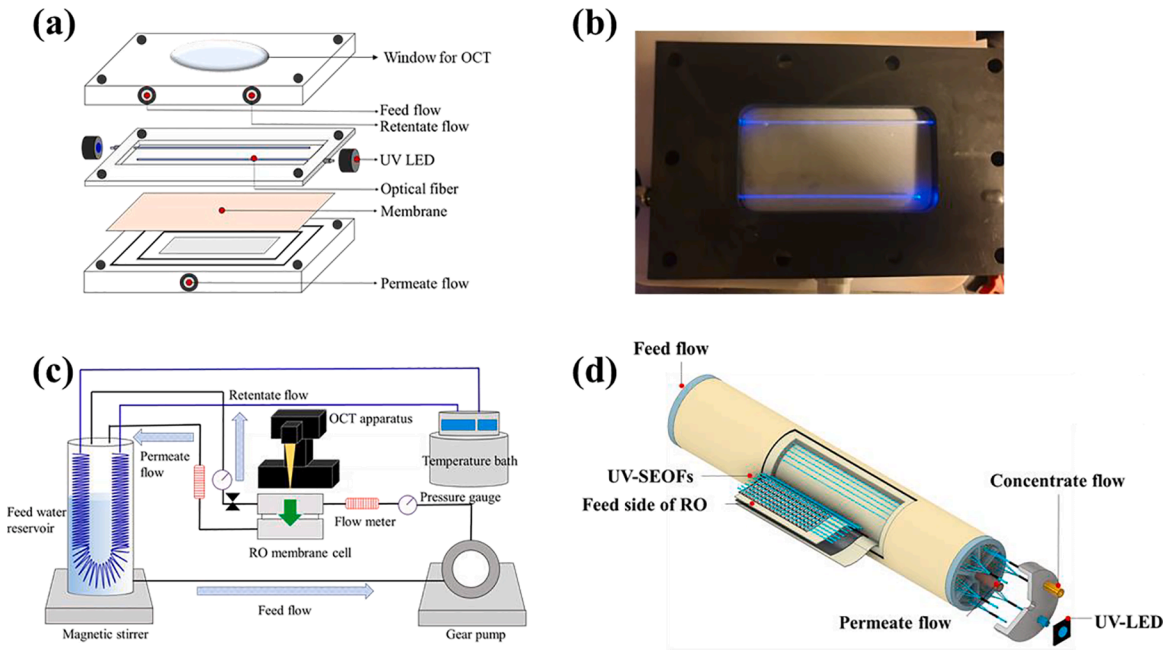

Fig. 1. RO membrane apparatus equipped with two SEOFs: (a) schematic of the membrane cell fully-enclosed with water cross-flow through the chamber, (b) photograph of two SEOFs connected to a functioning LED that is located outside the membrane cell chamber, (c) schematic of the membrane cell configured within a temperature-controlled recirculating system, (d) visualization of one concept to integrate flexible SEOFs as spacers within spiral-wound RO membrane modules.

systems were separately evaluated using a lab-scale cross-flow RO unit at a cross-flow velocity of 0.35 cm·s^{-1} using 10 L of synthetic wastewater as feed water under recirculation mode with 5 bar pressure for 8 d. Table SI-1 shows the characteristics of the feed water (*i.e.,* synthetic wastewater), which has an ionic strength of 15.9 mM and 40 mg L^{-1} of organic carbon substrate (glucose) (Rice et al., 2018); analytical grade NaCl, $MgSO_4{\cdot}7H_2O$, $NaHCO_3$, $CaCl_2{\cdot}2H_2O$, KH_2PO_4, NH_4Cl, and $Na_3C_6H_5O_7{\cdot}2H_2O$ were purchased from Sigma–Aldrich (St. Louis, MO, USA). The initial bacteria inoculum was $5{\times}10^8$ colony forming units (CFU)•mL^{-1} using a culture of *Pseudomonas aeruginosa* (ATCC 15692). *P. aeruginosa* was selected as a model microorganism, because it is among the most common biofilm-producing bacteria (Herzberg et al., 2009; Miller et al., 2012; Rice et al., 2018). Working with a single culture also facilitates interpretation of transcriptomic analysis. This proof-of concept study (i.e., Technology Readiness Level (TRL) 3-4) was designed to demonstrate viability and elucidate biofilm inhibition mechanisms using by UV-C and UV-A SEOFs.

Deionized (DI) water was added to the membrane coupon for 2 h before applying feed water to ensure membrane compaction. Continuous flux rates were measured gravimetrically using a scale (MS3002S/03, Mettler-Toledo, OH, USA), and real-time fouling layer formation was monitored by OCT (Thorlabs, Germany) using the Fourier-domain scanning technique at a relatively high scanning rate (30 kHz) (Im et al., 2021). To calculate salt rejection, the ion concentrations in the feed and permeate were measured using a conductance meter (Orion Versa Star Pro Advanced Electrochemistry Meter, Thermo, WA). Permeate water flux (J_w), and rejection (%) were calculated as follows:

$$\textit{Permeate flux}\ \left(J_w,\ \mathrm{L\ m^{-2}h^{-1}}\right) = \frac{V}{A} \tag{1}$$

$$\textit{Rejection}\ (\%) = \left(1 - \frac{C_p}{C_f}\right) \times 100 \tag{2}$$

where V is the permeate flow (L·h^{-1}), A is the membrane surface area (m^2), and C_f and C_p are the salt concentrations in the feed and permeate, respectively. The fouled RO membranes were collected after 8 d of cross-flow and further analyzed using various techniques described below.

2.3. Materials and fabrication method for SEOFs

Multimode optical fibers (diameter 1 mm, numerical aperture 0.39, core refractive index (RI) 1.5, high-OH: 300–1200 nm, model FT1000UMT) were purchased from Thorlabs (Newton, NJ, USA). Aminated silica sphere nanoparticles (SiO_2) suspended in 99.99% ethanol were obtained from NanoComposix (San Diego, CA, USA) and used as scattering centers. CyTop™ was used as a low UV-C absorbing polymer (CyTop™, BELLEX International Corp, Wilmington, DE, USA).

The fabrication steps of the UV-C and UV-A SEOFs for disinfection and photocatalytic oxidation are illustrated in Fig. SI-1. Detailed fabrication steps for the SEOFs were reported in our previous studies (Lanzarini-Lopes et al., 2019; Lanzarini-Lopes et al., 2020; O'Neal Tugaoen et al., 2018). Briefly, fiber optic segments (9 cm) were cut with a ceramic blade to obtain a smooth and flat cut surface. The polymer cladding on the fibers was manually removed using a specialized microstripper. The stripped fibers were then soaked in acetone for 15 min to dissolve the polymeric cladding, which is a thin coating that maintains the total internal light reflection. The uncoated fibers were subsequently rinsed and cleaned with nanopure water. The optical fiber segments were individually fixed to metallic LED connectors (SMO5SMA, Thorlabs) using the heat-shrink wrap. The fibers were mounted on a fiber support (D50SMA, Thorlabs), and the cut surface was polished with optical polishing paper (LF30P, LF5P, and LF03P) until a specular surface was obtained. Both ends of each optical fiber were polished to maximize light entrance from the LED into the fiber. These fibers were then coated to enable side emission of UV-C or UV-C light, plus ROS production by surface activation when TiO_2 was present as a photocatalysts.

Following prior detailed SEOF fabrication methodologies published elsewhere, UV-C SEOFs were prepared by aminated silica nanoparticles (SiO_2) coating onto stripped optical fibers through electrostatic attraction using dip-coating for 60 s followed by air drying for 5 min (Zhao et al., 2021). The fibers were then dipped in polymer solution and dried in air for 2 h. A previous study confirmed that CyTop™ has negligible attenuation, light scattering, and reflection (Lanzarini-Lopes et al., 2019).

For UV-A SEOFs, the TiO_2 P90 photocatalyst (Sigma Aldrich) was deposited on the fiber surface using a dip-coating method (Ling et al.,

2017). A 1.0% TiO_2 P90 dispersion (10 g•L^{-1}) was prepared according to a previously published protocol (Tantra et al., 2015). The dispersion solution was prepared in nanopure water and sonicated using a QSonica Misonix immersion sonicator for 15 min. The optical fibers were immersed in the dispersion solution for 60 s and then slowly removed from the dispersion solution. Subsequently, the coated fibers were heat-dried at 100°C for 5 min to ensure TiO_2 adhesion to the optical fiber surface.

2.4. Analytical methods

To confirm side-emission, the light intensity (265 nm and 365 nm) along the SEOFs was analyzed using a spectrophoto-radiometer (calibration: 200–1100 nm; Avantes, Louisville, CO, AvaSpec-2048 L) at different lengths along the fiber (L = 1–9 cm) following previously-described methods (Zhao et al., 2021). To confirm hydroxyl radical (•OH) production from UV-A SEOFs, experiments were performed using a solution para-hydroxybenzoic acid (*p*-HBA) from 1 μM benzoic acid (Klein et al., 1975). Because the benzoic acid reacts with •OH to form three hydroxybenzoic acid isomers (ortho, meta and para hydroxybenzoic acid, in a ratio of 1.7:2.3:1.2), the hydroxyl radical production was confirmed by quantifying *p*-HBA.

Membrane surface properties of the virgin and fouled RO membranes were determined; zeta potential was measured using the streaming potential MCR 102, Anton Paar GmbH, Graz, Austria) in a 10 mM KCl electrolyte solution, and contact angle (*i.e.,* hydrophobicity) was measured using a goniometer (Attension Theta by Biolin Scientific, Gothenburg, Sweden).

At the end of each membrane test, the biofilms were characterized. First, bacterial deposition on the fouled RO membranes was quantified using a CFU assay. To detach bacteria from the surface, the fouled membranes were gently washed in synthetic wastewater, placed in 15 mL Falcon tubes filled with 5 mL of synthetic wastewater, and bath sonicated for 6 min to remove cells without compromising viability (Frank et al., 2017). A 0.1 mL volume of the solution in the Falcon tube was withdrawn and diluted with distilled (DI) water at 1:100. The 1:100 solution was plated on LB agar plates in 50 μL aliquots, placed in an incubator, and allowed to grow overnight. CFU counts were determined the following day.

Second, live/dead cell viability was determined using a Leica DM6 fluorescence microscope (Leica Microsystems Inc. Buffalo Grove, IL) after the injection of 3 mL of 3.34 mM Syto9 and 3 mL of 4.67 mM propidium iodide (Molecular Probes, Carlsbad, CA) into each flow channel to stain live and dead cells in green and red, respectively. Images were analyzed using ImageJ software (National Institutes of Health, MD, USA) to determine live cell viability.

Third, the phenol–sulfuric acid method (Dubois et al., 1956) and a Micro BCA™ Protein Assay Kit (Thermo Scientific, Waltham, MA, USA) was used to determine EPS concentration (*e.g.,* polysaccharides and proteins) from the supernatants based on the calibration curves between concentration and UV absorbance (Fig. SI-2).

Fourth, quantifying the gene expression of bacterial deposition on the fouled membranes involved quorum sensing (QS; *i.e., lasI/R* and *rhlI/R*), polysaccharide synthesis (*i.e., pelA* and *pslA*), surface attachment (*i.e., cdrA* and *sagS*), and oxidative stress response (*i.e., msrB, sodM*, and ospR). Real-time quantitative PCR (RT-qPCR) was performed in 15 μL of reaction mixture composed of 2 ng of cDNA, SYBR Green Master Mix (7.5 μL), each primer at 0.3 μM, and water, using the housekeeping gene *recA* as an internal standard (Dietrich et al., 2006; Livak and Schmittgen, 2001; Ma et al., 2006; Winsor et al., 2010; Yang and Alvarez, 2015).

3. Results and discussions

3.1. Characterization of side emission and photocatalytic activity of UV-C versus UV-A SEOFs

Homogeneous distribution of SiO_2 and TiO_2 on the surfaces of the UV-C and UV-A SEOFs, respectively, was confirmed using scanning electron microscopy (images shown in Fig. SI-3). X-ray diffraction (XRD) spectra of TiO_2 (P90) powder, the pristine optical fiber, and UV-A SEOFs confirmed TiO_2 was present on the coated fiber and that anatase was the dominant phase; anatase is photocatalytic when exposed to 365 nm light as shown in Fig. SI-4.

Light was uniformly emitted from the side of the optical fibers along their length. Fig. 2a shows side-emitted light fluence. Thus, the nanoparticle coatings were effective at delivering light to the surface of the SEOFs. Despite applying the same current (0.45 amp) to the 265 nm and 365 nm LEDs, the side-scattered light for the UV-A SEOF averaged ~100 μW·cm^{-2} (89–200 μW·cm^{-2}) and was higher than the 10 μW·cm^{-2} average (6–10 μW·cm^{-2}) from the UV-C SEOF. This is because the UV-A LEDs have higher wattage and because the longer wavelength LEDs are more efficient at producing light rather than heat (Loeb et al., 2018). Light fluence was slightly higher at the proximal end of SEOFs because it was nearer to the LED and because of back-refracted light still being transmitted within the SEOF. Prior research showed that >2 μW·cm^{-2} of UV-C light delivered by SEOFs inactivates *Pseudomonas aeruginosa* and *Escherichia coli*, even on very nutrient-rich surfaces (Lanzarini-Lopes et al., 2019). Additionally, our prior research showed that flux and salt rejection of RO membranes are not compromised until UV doses much above 25 J·cm^{-2} (*i.e.,* potentially years of operation in our envisioned system) (Rho et al., 2021). Therefore, UV-C light is not expected to impact the RO membrane performance over the duration of the current experiments in the absence of bacteria (further discussed later).

For the 365 nm LED and TiO_2-coated SEOF, the photocatalytic behavior was demonstrated by oxidation by •OH of benzoic acid (BA) to *p*-HBA. Fig. 2b shows no *p*-HBA for a non-coated optical fiber attached to the UV-A LED, whereas *p*-HBA formation increased gradually over time for the TiO_2-coated SEOF. The previous study clearly revealed that BA acts as an •OH scavenger, but not as a hole scavenger (Kim et al., 2015). Therefore, BA can only be transformed to *p*-HBA by the •OH and this result validated the potential for the TiO_2-coated SEOF to produce •OH.

3.2. Mitigation of biofilm-induced flux decline using UV-C versus UV-A SEOFs

Fig. 3 shows water flux and salt rejection during control and UV irradiation experiments over 8 d with a recirculating feed solution containing *P. aeruginosa*. The control experiment had SEOFs in the membrane cell, but no LEDs were attached (*i.e.,* no irradiation on SEOFs and thus only hydrodynamic influences). The aim was to study surface mitigation of biofouling. By using a common large volume of recirculating feed water containing bacteria for both control and UV-irradiated membrane cells, any inactivation or stress to planktonic bacteria would be experienced by both membrane cells. Planktonic bacteria were expected to be continuously deposited onto the membrane surfaces, even in the presence of UV irradiation from the SEOFs. Control and UV irradiation experiments each had the same initial permeate flux (11.5 L·m^{-2}·h^{-1}).

Fig. 3a shows the normalized permeate flux of all three RO experiments decreased over time, indicating that some biofouling likely occurred on the RO membrane surfaces (Herzberg and Elimelech, 2007). Control experiments showed the fastest and largest flux decline, consistent with many other similar membrane cell studies that attribute flux decline to surface biofilm formation. The decline in permeate flux was slower when SEOFs were connected to LEDs. The results were highly reproducible, as evident by small error bars on flux decline tests from duplicate experiments. The UV-C SEOF exhibited a faster initial

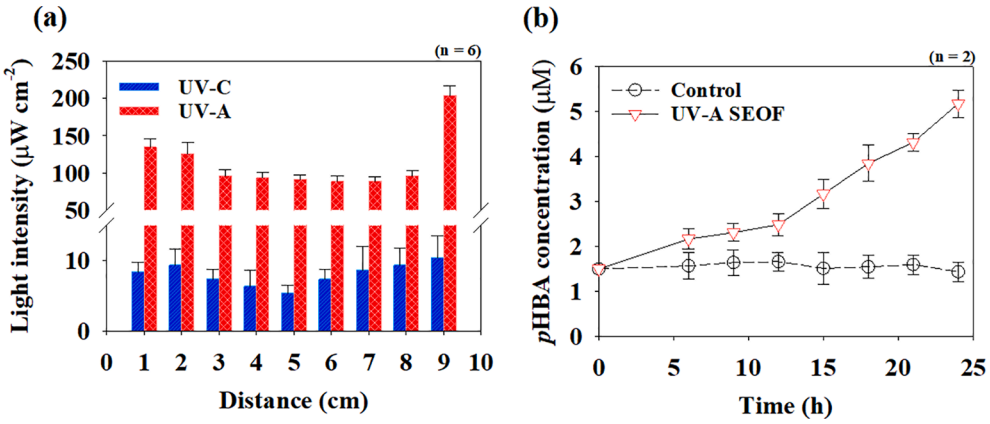

Fig. 2. Performance of the UV-C and UV-A SEOFs: (a) distributions of UV-C and UV-A light intensity along fiber length, (b) quantity of •OH produced from UV-A SEOFs using *p*-HBA method.

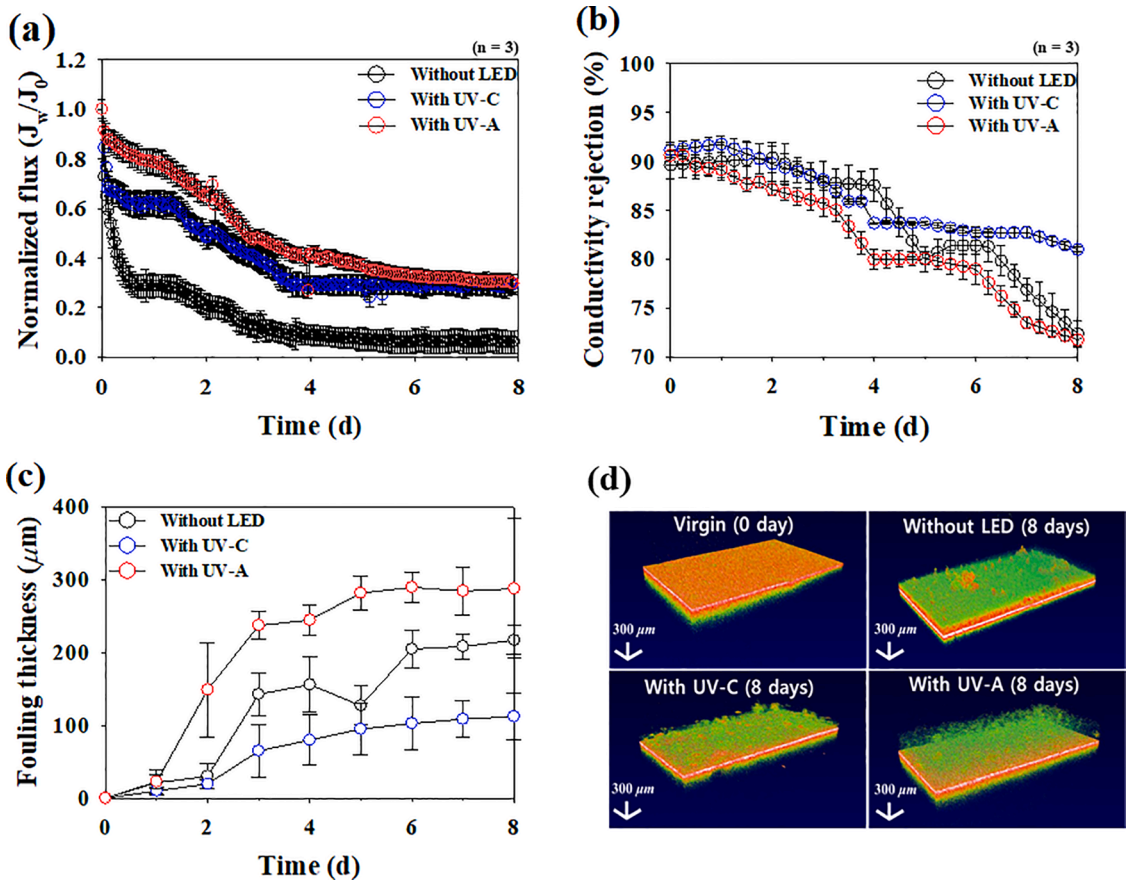

Fig. 3. Biofouling propensities of lab-scale RO membrane unit with UV-A and UV-C LED and without LED: (a) Flux decline during 8 d by biofouling, (b) salt rejections during 8 d of operation, (c) thickness of fouling layer measured by OCT, (d) 3-dimensional images of RO membrane surfaces after 8 d obtained from OCT.

flux decline compared against the UV-A SEOF experiment, but then the UV-C SEOF showed a slower rate of flux decline over the remaining 8 d. This suggests a steady-state surface biofilm formation. A continuous flux decline over time was observed with the UV-A SEOF. After 8 d, the UV-A and UV-C SEOF experiments both had similar flux declines ($J_w/J_0 \sim 0.4$) that indicated less biofouling than the control ($J_w/J_0 < 0.1$). Because planktonic bacteria were present in the recirculating nutrient-rich feed solution, we did not expect to "sterilize" the membrane surfaces with the SEOFs. Rather, we expected only to achieve less decline in permeate flux associated with somewhat constant attachment/detachment of bacteria from the membrane surface (Reid et al., 2014). This appeared to be attained for the UV-C SEOF, based on permeate fluxes.

Fig. 3b shows changes in salt rejection over time for control and the SEOF experiments. Similar losses in salt rejection were observed over the first few days, after which the UV-C SEOF maintained higher salt rejection than the control or UV-A SEOF. Two possible reasons explain the decreased salt rejection: (i) ROS generated by UV-A SEOFs can pass through the biofouling layer, damage the membrane surface, and thereby lead to detrimental effects on membrane performance (Nasrollahi et al., 2021) or (ii) the surface charge of the RO membrane can be reduced by bacterial deposition, leading to decreased Donnan exclusion effects (Rho et al., 2020; Rho et al., 2019). The loss in salt rejection was

greatest for the UV-A SEOFs, slightly more so than the membrane cell without any UV light exposure. The highest permeate water production was observed with UV-A SEOFs when compared to UV-C SEOFs and control experiments. Accordingly, it can be postulated that the RO membrane surface was slightly compromised by ROS generated from UV-A SEOFs passing through a loosely formed fouling layer. Additional control experiments performed using an RO membrane equipped with UV-A SEOFs/TiO_2 was conducted using 10 mM of NaCl solution as a feed water (without bacteria) to investigate the membrane could be damaged by ROS generated from UV-A SEOFs. Results showed that permeate water flux and conductivity rejection of RO membrane gradually increased and decreased, respectively, at rates above those observed in the presence of biofilms on the membrane surface as shown in Fig. SI-5 (R_t/R_0 with biofouling: 81.6%; R_t/R_0 without biofouling: 21.4%). Thus, these results imply that the loosely attached biomass on the fouled RO membrane equipped with UV-A TiO_2/SOEFs produce allows ROS to pass through biofouling layers, reach the membrane surface, and adversely impact RO membrane performances.

The biofouling layers was monitored in real-time by OCT during the RO membrane operation (Fig. SI-6), and the biofilm layer thickness was estimated from the OCT images (Fortunato et al., 2017). Fig. 3c shows changes throughout each experiment. It was expected that UV irradiation would decrease the biofilm thickness. Unexpectedly, the biofilm layer after 8 d was thicker on the membrane with the UV-A photocatalytic SEOFs (287 ± 95.7 μm) compared against the control membrane without UV irradiation (217 ± 19.6 μm). However, the thinnest biofilm layer was observed in the membrane cells equipped with UV-C SEOFs (103 ± 31.7 μm). Furthermore, Fig. 3d shows 3-dimensional OCT images of the RO membrane surface after 8 d, with a relatively loose, low density, rough biofilm layer observed for the UV-A SEOFs, compared against a more compact biofilm layer on the control and UV-C SEOF membrane cells.

Overall, biofouling was significantly influenced by the photocatalytic oxidation or disinfection from UV-A and UV-C SEOFs. UV-A SEOFs promoted formation of a less dense but thicker biofouling layer, and the ROS generated from UV-A SEOFs may have passed through the less-dense biofouling layer and degraded the polymeric RO membrane surface. UV-C SEOFs had less loss of permeate flux (*i.e.,* less biofouling) than the control and retained the highest salt rejection. UV-C SEOFs also performed the most consistently (*i.e.,* least change in permeate flux or salt rejection over 8 d), which corresponds logically to the membrane cell with the least influence from biofilms (*i.e.,* thinnest biofilm layer – Fig. 3c). Moreover, SEOFs are stable under 5 bar of pressure in RO unit over 8 d. Because, glass optical fiber basically has a high tensile strength of 5×10^3 N/mm^2, approximately 53,000 bar, indicating that SEOFs have very strong mechanical properties. Additionally, SEOFs are flexible enough due to their transparent polymer coating as shown in Fig. SI-7.

3.3. Characterization of changes in RO membrane surfaces after exposures using UV-C versus UV-A SEOFs

Fig. 4a shows zeta potential of virgin and fouled membranes (from control or UV SEOF experiments). The virgin and fouled RO membranes showed negatively zeta potentials over most of the pH range. The amphoteric curves are associated with the carboxyl and amine functional groups attached to the RO membranes, as generally observed in previous studies (Rho et al., 2018). Furthermore, the surface zeta potentials of the RO membrane became less negatively charged as the biofouling layer formed on the membranes; UV-A > without LED > UV-C (without LED at pH 7 was -7.3 ± 1.5 mV, UV-C at pH 7 was -9.1 ± 2.2 mV, and UV-A at pH 7 was -3.4 ± 1.3 mV). This likely indicates larger biofoulant accumulation on RO membrane equipped with UV-A SEOFs than the control. The $^{\bullet}$OH generated by UV-A SEOFs may be promoting biofoulant accumulation near the membrane surface (Cai and Liu, 2016; Pemmaraju et al., 2016).

Surface contact angles of the virgin and fouled RO membrane surfaces are shown in Fig. 4b. Virgin RO membrane shows the highest contact angles (40 ± 3°), consistent with prior measurements (Rho et al., 2021). In the control tests, biofouling rendered the RO membrane surface more hydrophilic (*i.e.,* 29 ± 4°). UV-C SEOFs resulted in a surface contact angle (35 ± 2°) closer to the virgin membrane (40 ± 3°) than the control membrane system (29 ± 4°). UV-A SEOFs resulted in a surface with the lowest contact angle (25.2 ± 1.9°). Some biofilms existed in both control (no light) and experiments with UV irradiation experiments. Membrane surface characterization provides additional insights into the nature of foulants (Lee et al., 2010), but in both causes after 8 days of operation both the underlying membrane and surface biofilms influence surface properties. Changes in zeta potential and surface contact angle measures (Fig. 4) coincided with biofilm thickness (Fig. 3c). The presence of thicker biofilms resulted in larger changes in these surface measurements, because the biofilms themselves exerted a stronger effect on the measurements relative to the native surface properties of the underlying RO membrane.

3.4. Biological and chemical composition of membrane foulants

To support *in-situ* OCT measurements of biofilm density over time, after 8 d the membrane cell was opened and biomass was collected from nine regions distributed across the membrane surface. Fig. SI-8 schematically illustrates sample locations that were then used to create surface contour plots (Fig. 5) for various measurements by assigning a measured concentration to each of these nine regions on the membrane

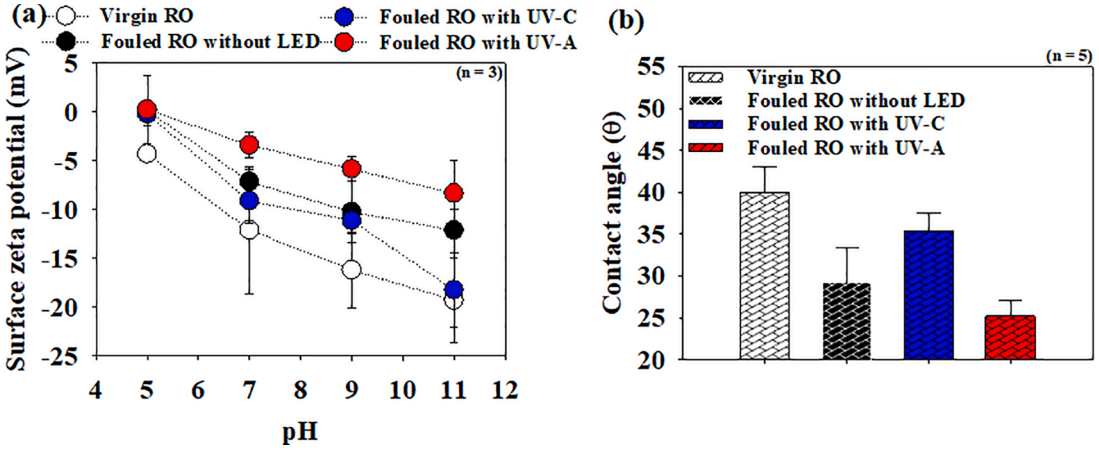

Fig. 4. Surface properties of virgin and fouled RO membranes: (a) surface zeta potential measured in 10 mM of KCl electrolyte solution, (b) contact angle of RO membrane measured using 10 μL of DI water.

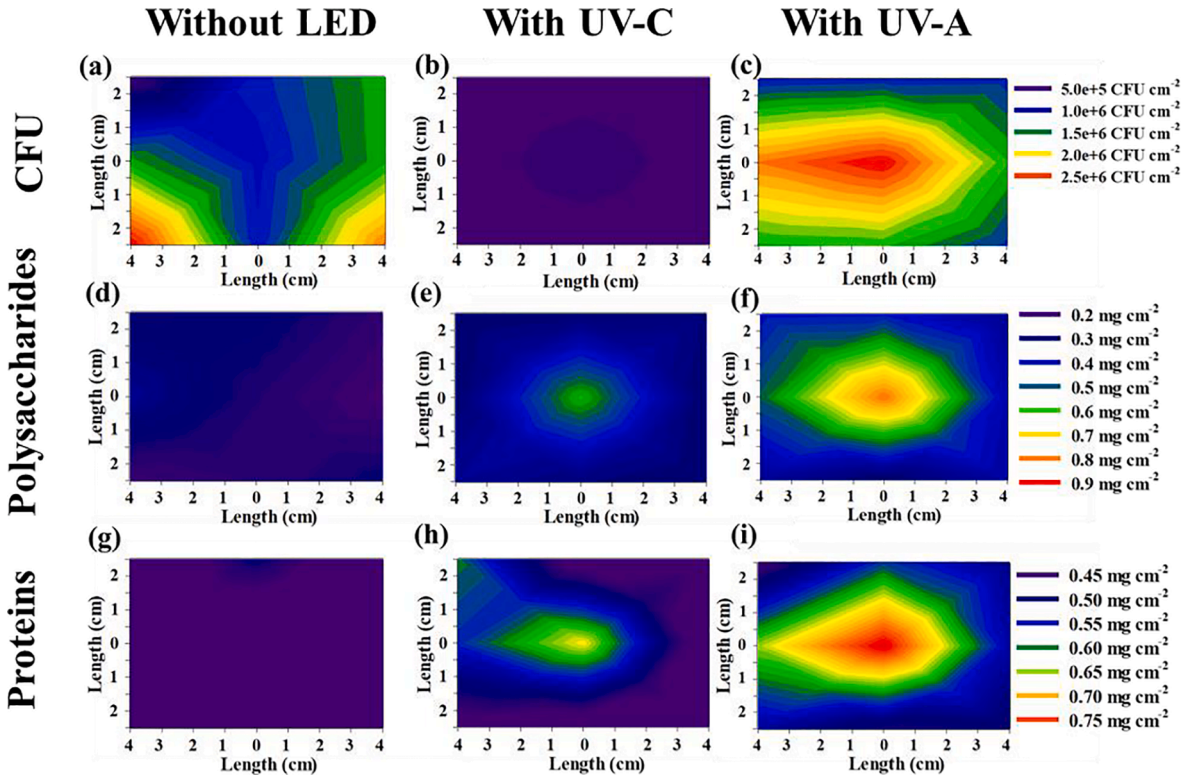

Fig. 5. Accumulated biomass on the membrane surface divided into nine zones using typical CFU counts and EPS measurements after membrane fouling: CFU counts from fouled RO membranes (a) without LED, (b) with UV-C SEOFs, and (c) with UV-A SEOFs; polysaccharides substances extracted from fouled RO membranes (d) without LED, (e) with UV-C SEOFs, and (f) with UV-A SEOFs; protein substances extracted from fouled RO membranes (g) without LED, (h) with UV-C SEOFs, and (i) with UV-A SEOFs.

surface (*i.e.,* length and width plotted on x- and y-axis). Fig. 5a–c show differences in CFU for the control, UV-C SEOF, and UV-A SEOF experiments, respectively. Across all nine regions (Fig. 6), bacterial counts averaged 1.6×10^6, 0.8×10^4, and 1.3×10^6 CFU·cm^{-2} for the control, UV-C SEOF, and UV-A SEOF experiments, respectively. Bacterial counts were not uniform across the membrane surface but were less than 1 log difference in CFU/mL across the membrane. Consistent with OCT measurements, UV-C SEOF experiments showed the lowest biofilm accumulation and had a maximum CFU/mL of $\sim 2 \times 10^4$/mL, which is ~2 log lower than the maximum bacterial counts for the control or UV-A SEOF systems ($\sim 2.5 \times 10^6$/mL).

Based on staining and confocal images obtained from the fluorescence microscope (Fig. SI-9), Fig. 6 shows that UV-C SEOF experiments exhibited the lowest live-cell viability (18%), followed by 60% viability for UV-A SEOFs and 71% viability in control experiments. These results are consistent with CFU/mL data, showing the largest impact by UV-C SEOFs.

Using the same 9 sample locations as for bacteria concentrations (CFU·cm^{-2}, Fig. 5d–f and 5g–i show data for EPS components (polysaccharides and proteins, respectively). EPS concentrations were lowest for the control and highest for the UV-A SEOFs, with UV-C SEOFs in the middle. Polysaccharide and protein concentrations had similar orders of magnitude (0.1 to 1 mg·cm^{-2}) and exhibited similar spatial patterns across the membrane surface. As shown in Fig. 6c, the amounts of EPS per unit cell were highest for the UV-A SEOFs compared to others, implying that ROS generated from UV-A SEOFs promote to bacterial cells to secrete EPS. Data in Fig. 5 suggest different spatial patterns in biofilm growth for the control versus UV-irradiated membranes.

Control experiments appeared to have highest biofilm density around the outside walls of the membrane cell, whereas the irradiated membranes had the highest density in the center of the membrane cell. Control experiments had SEOFs without irradiation, so these patterns are unlikely associated with differences in hydrodynamics within the membrane cells. Instead, we postulate that the spatial patterns were associated with bacterial responses to UV-C light or UV-A photocatalytically-produced ROS.

To investigate how bacteria are responding to UV-C irradiation or $^{\bullet}$OH generated by UV-A, biofilm samples were subjected to

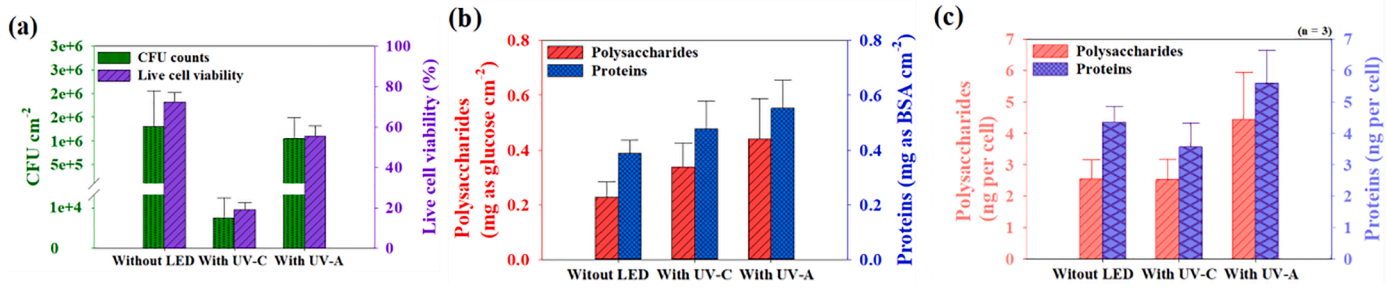

Fig. 6. Characteristics of biofoulants eluted from fouled RO membranes: (a) CFU counts and live-cell viability, (b) EPS quantification, (c) EPS per unit cell (ng/cell).

transcriptomic analysis (Yang and Alvarez, 2015). Overall, UV-C and UV-A SEOFs induced the expression of *P. aeruginosa* genes associated with biofouling formation on RO membranes. *P. aeruginosa* generally contains two quorum sensing (QS) systems, *las* and *rhl*, and either system consists of one transcriptional activator (*lasR* or *rhlR*) and an auto-inducer synthase (*lasI* or *rhlI*). The *las* system dominates and controls the *rhl* system, whereas the two systems are linked. Fig. 7 shows up or down regulation of several genes relative to control experiments (*i.e.*, without UV irradiation). UV-C SEOFs induced *lasI* (4.2 ± 1.6-fold), *lasR* (6.4 ± 1.2-fold), *rhlI* (0.3 ± 0.7-fold), and *rhlR* (1.0 ± 1.3-fold), while *lasI* (-3.3 ± 1.2-fold), *lasR* (-1.1 ± 1.1-fold), *rhlI* (-2.9 ± 2.5-fold), and *rhlR* (-2.7 ± 1.6-fold) were down-regulated by UV-C SEOFs. Separately, UV-A SEOFs upregulated expression of polysaccharides synthesis gene *pelA* (4.2 ± 1.1-fold) and *pslA* (2.1 ± 0.6-fold) and induced expression of surface attachment gene *cdrA* (3.4 ± 1.3-fold) and *sagS* (4.1 ± 1.0-fold), while both expressions of polysaccharides synthesis and surface attachment genes were down-regulated by UV-C SEOFs (*pelA*: 0.7 ± 0.7-fold; *pslA*: -0.3 ± 1.6-fold; *cdrA*: -1.1 ± 0.9-fold; *sagS*: -3.2 ± 1.3-fold).

Both UV-C and UV-A SEOFs induced expression of oxidative stress response. For UV-C SEOFs, the responses were as follows: *msrB* = 2.7 ± 0.5-fold; *sodM* = 1.8 ± 0.3-fold; *ospR* = 3.4 ± 0.8-fold. For UV-A SEOFs the responses were as follows: *msrB* = 4.8 ± 1.7-fold; *sodM* = 5.5 ± 1.4-fold; *ospR* = 4.1 ± 1.1-fold. The photocatalytic UV-A SEOFs had significantly more effect on the oxidative stress response.

Stimulation of QS, polysaccharide synthesis, surface attachment, and oxidative stress response corroborates the observation that a low level of $^{\bullet}$OH generated by the UV-A SEOFs may promote formation of biofilm, secretion of more EPS to protect microorganism growth, and resistance to oxidative stress (Chen et al., 2022; Pezzoni et al., 2018). Higher $^{\bullet}$OH generation may be more effective for microbial inactivation (Wang et al., 2015); however, UV-C SEOFs that directly deliver germicidal irradiation (2 to 10 μW·cm^{-2}) to the membrane surface are sufficient to inhibit biofouling formation, affecting the expression of QS regulation and surface attachment genes. This is because aromatic heterocyclic pyrimidine bases in DNA are dominant absorbers of UV light, while ROS generated by photocatalysis are non-selective, oxidizing whole cell constitutes. Overall, these results suggest superior performance of UV-C SEOFs relative to UV-A SEOFs to mitigate the detrimental effects of biofouling on membrane performance.

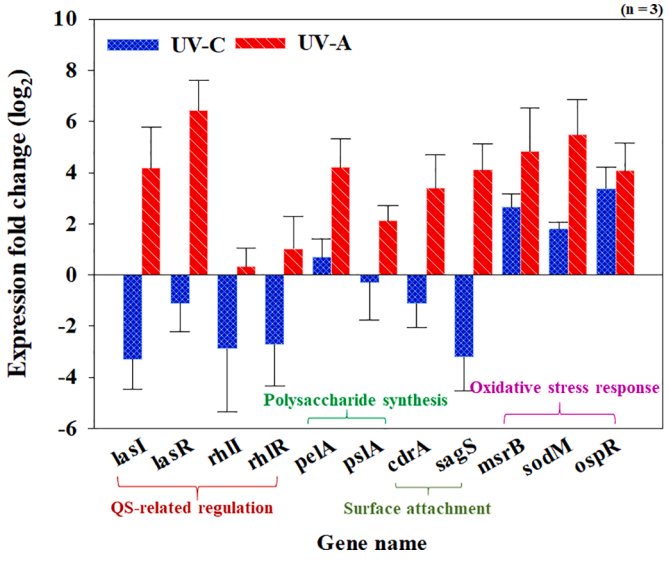

Fig. 7. Transcriptomic analysis for *P. aeruginosa* exposed to UV-C and UV-A SEOFs. Error bars represent ± one standard deviation from the mean of triplicate measurements.

4. Conclusions

We demonstrated that an RO membrane unit equipped with UV-C SEOFs effectively inhibited *P. aeruginosa* growth on membrane surfaces, mitigating adverse performance decline in water flux otherwise associated with biofouling. The thin and flexible UV-C SEOFs resulted in some, but relatively thin and less dense biofilms on the membranes compared to parallel systems that did not launch UV-C light into the SEOFs. Of significant importance is that UV-C SEOFs resulted in more constant performance (*i.e.,* slower rate of change over time in permeate flux or salt rejection) than control experiments where biofilms grew on the membrane surface.

UV-A irradiated TiO_2-coated SEOFs continuously generated $^{\bullet}$OH concentrations that were insufficient to prevent inhibit bacterial growth on RO membrane surfaces. In fact, $^{\bullet}$OH generated from UV-A SEOFs coated with TiO_2 promoted microorganism attachment to the membrane surface, resulting in thick fouling layers with significant amounts of EPS, possibly as a hermetic response to sublethal stress. It is possible that the $^{\bullet}$OH oxidized organics in the feed water or within the biofilm matrix into more readily biodegradable materials, which promoted biofilm growth. OCT imaging of biofilm density on the membranes showed biofilms were loosely attached on the fouled RO membrane equipped with UV-A SEOFs compared to the others, allowing ROS to pass through biofouling layers, reach the membrane surface, degrade the polymer and adversely impact sustainable RO membrane performances.

Transcriptomic analysis results revealed that UV-C SEOFs down-regulated quorum sensing and surface attachment genes. In contrast, UV-A SEOFs upregulated quorum sensing, surface attachment, and oxidative stress genes, resulting in higher EPS accumulation on membrane surfaces. This occurred because aromatic heterocyclic pyrimidine bases in DNA are dominant absorbers of UV light, while ROS generated by photocatalysis are non-selective, oxidizing whole cell constitutes. Apparently, $^{\bullet}$OH concentrations within the reactors promoted biofilm formation by producing more EPS in response to the oxidative stress conditions, in an attempt to protect *P. aeruginosa*. Consequently, the best performing wavelengths were UV-C wherein the SEOFs resulted in less loss of permeate flux than the control and maintained the highest salt rejection.

While there is potential for UV-C light to damage polyamide RO membranes, ongoing experiments in our laboratory suggests continuous irradiation may not be required to control biofilm growth. If the UV exposure or dose (μW·cm^{-2} × time) achieve surface bacterial inactivation rates greater than bacterial growth rates, then biofilm growth may be inhibited. Therefore, we are exploring "duty-cycling" wherein LEDs are cycled on for a short period of time and then off for 5 to 50 times longer than the on cycle. This lengthens the operation time to several years before accumulated doses even approach levels (*i.e.,* > 25 J·cm^{-2}) previously found to cause membrane defects to polymer surfaces (Rho et al., 2021).

UV-SEOFs represent an emerging non-chemical strategy to mitigate biofouling and reduce operational costs associated with RO treatment and demonstrated its potential to improvement membrane performance. Thin and flexible SEOFs may incrementally increase in capital costs of RO modules (*e.g.,* as RO membrane spaces), and require very low powered (< 100 mW) UV light from LEDs attached to the SEOFs. The tradeoff against increase pressure to maintain water flux and/or down-time plus chemical usage is likely to be reduces through integration of UV-SEOFs into RO modules. Our experiments applied relatively high bacterial and nutrient concentration in the feed solution, relative to pretreated water in wastewater reuse facilities. While future research on such wastewaters will be needed, the model feed waters and organisms used in our study are commonly used to elucidate biofouling inhibition (Jiang et al., 2022; Liu et al., 2022; Ni et al., 2021; Qiu et al., 2022; Torkzadeh et al., 2021). We are currently attempting to fabricate spiral-wound RO membrane modules (*e.g.,* as shown in Fig. 1d) with SEOFs integrated as RO membrane spacers, and performing longer-term

biofouling inhibition studies using microfiltered wastewater or seawater as feed water. This type of experimental data will be integrated into techno-economic analysis to quantify system costs tradeoffs and benefits of integrating UV-SEOFs to develop a new generation of non-chemical biofouling inhibition strategies for sustainable membrane processes.

Declaration of Competing Interest

The authors declare that they have no known competing financial interests or personal relationships that could have appeared to influence the work reported in this paper.

Data Availability

Data will be made available on request.

Acknowledgments

This work was partially funded by the National Science Foundation (EEC-1449500) Nanosystems Engineering Research Center on Nanotechnology-Enabled Water Treatment and NASA (80NSSC19C0564). This work also supported by Korea Ministry of Environment (MOE) as "High-purity industrial water production process localization development program (2021003230002)" and used facilities within the Eyring Materials Center at Arizona State University supported in part by the National Science Foundation (NNCI-ECCS-1542160). Laurel Passantino provided technical editing.

Supplementary materials

Supplementary material associated with this article can be found, in the online version, at doi:10.1016/j.watres.2022.119094.

References

Bar-Zeev, E., Passow, U., Romero-Vargas Castrillón, S., Elimelech, M., 2015a. Transparent exopolymer particles: from aquatic environments and engineered systems to membrane biofouling. Environ. Sci. Technol. 49 (2), 691–707.
Bar-Zeev, E., Perreault, F., Straub, A.P., Elimelech, M., 2015b. Impaired performance of pressure-retarded osmosis due to irreversible biofouling. Environ. Sci. Technol. 49 (21), 13050–13058.
Beck, S.E., Hull, N.M., Poepping, C., Linden, K.G., 2018. Wavelength-dependent damage to adenoviral proteins across the germicidal UV spectrum. Environ. Sci. Technol. 52 (1), 223–229.
Beck, S.E., Rodriguez, R.A., Hawkins, M.A., Hargy, T.M., Larason, T.C., Linden, K.G., 2016. Comparison of UV-induced inactivation and RNA damage in MS2 phage across the germicidal UV spectrum. Appl. Environ. Microbiol. 82 (5), 1468–1474.
Beck, S.E., Ryu, H., Boczek, L.A., Cashdollar, J.L., Jeanis, K.M., Rosenblum, J.S., Lawal, O.R., Linden, K.G., 2017. Evaluating UV-C LED disinfection performance and investigating potential dual-wavelength synergy. Water Res. 109, 207–216.
Bolton, J.R., Cotton, C.A., 2011. The Ultraviolet Disinfection Handbook. American Water Works Association.
Cai, W., Liu, Y., 2016. Enhanced membrane biofouling potential by on-line chemical cleaning in membrane bioreactor. J. Membr. Sci. 511, 84–91.
Chen, J., Loeb, S., Kim, J.H., 2017. LED revolution: fundamentals and prospects for UV disinfection applications. Environ. Sci. Water Res. Technol. 3 (2), 188–202.
Chen, M., Cai, Y., Li, G., Zhao, H., An, T., 2022. The stress response mechanisms of biofilm formation under sub-lethal photocatalysis. Appl. Catal. B 307, 121200.
Dietrich, L.E., Price-Whelan, A., Petersen, A., Whiteley, M., Newman, D.K., 2006. The phenazine pyocyanin is a terminal signalling factor in the quorum sensing network of Pseudomonas aeruginosa. Mol. Microbiol. 61 (5), 1308–1321.
Dotson, A.O., Rodriguez, C.E., Linden, K.G., 2012. UV disinfection implementation status in US water treatment plants. J. Am. Water Works Assoc. 104 (5), 77–78.
Dubois, M., Gilles, K.A., Hamilton, J.K., Rebers, P.t., Smith, F., 1956. Colorimetric method for determination of sugars and related substances. Anal. Chem. 28 (3), 350–356.
Flemming, H.C., Wingender, J., 2010. The biofilm matrix. Nat. Rev. Microbiol. 8 (9), 623–633.
Fortunato, L., Qamar, A., Wang, Y., Jeong, S., Leiknes, T., 2017. *In-situ* assessment of biofilm formation in submerged membrane system using optical coherence tomography and computational fluid dynamics. J. Membr. Sci. 521, 84–94.
Frank, H., Rahav, E., Bar-Zeev, E., 2017. Short-term effects of SWRO desalination brine on benthic heterotrophic microbial communities. Desalination 417, 52–59.
Freire-Gormaly, M., Bilton, A., 2019. Impact of intermittent operation on reverse osmosis membrane fouling for brackish groundwater desalination systems. J. Membr. Sci. 583, 220–230.
Herzberg, M., Elimelech, M., 2007. Biofouling of reverse osmosis membranes: role of biofilm-enhanced osmotic pressure. J. Membr. Sci. 295 (1), 11–20.
Herzberg, M., Kang, S., Elimelech, M., 2009. Role of extracellular polymeric substances (EPS) in biofouling of reverse osmosis membranes. Environ. Sci. Technol. 43 (12), 4393–4398.
Im, S.J., Fortunato, L., Jang, A., 2021. Real-time fouling monitoring and membrane autopsy analysis in forward osmosis for wastewater reuse. Water Res. 197, 117098.
Jafari, M., Vanoppen, M., van Agtmaal, J.M.C., Cornelissen, E.R., Vrouwenvelder, J.S., Verliefde, A., van Loosdrecht, M.C.M., Picioreanu, C., 2021. Cost of fouling in full-scale reverse osmosis and nanofiltration installations in the Netherlands. Desalination 500, 114865.
Jiang, T., Tian, T., Guan, Y.F., Yu, H.Q., 2022. Contrasting behaviors of pre-ozonation on ceramic membrane biofouling: early stage vs late stage. Water Res., 118702
Kim, J., Moon, G.H., Kim, S., Kim, J., 2015. Photocatalytic oxidation mechanism of arsenite on tungsten trioxide under visible light. J. Photochem. Photobiol. A 311, 35–40.
Klein, G.W., Bhatia, K., Madhavan, V., Schuler, R.H., 1975. Isomer distribution in the radical intermediates. J. Phys. Chem. 79 (17), 1767–1774.
Lanzarini-Lopes, M., Cruz, B., Garcia-Segura, S., Alum, A., Abbaszadegan, M., Westerhoff, P., 2019. Nanoparticle and transparent polymer coatings enable UV-C side-emission optical fibers for inactivation of escherichia coli in water. Environ. Sci. Technol. 53 (18), 10880–10887.
Lanzarini-Lopes, M., Zhao, Z., Perreault, F., Garcia-Segura, S., Westerhoff, P., 2020. Germicidal glowsticks: side-emitting optical fibers inhibit pseudomonas aeruginosa and Escherichia coli on surfaces. Water Res. 184, 116191.
Lee, W., Ahn, C.H., Hong, S., Kim, S., Lee, S., Baek, Y., Yoon, J., 2010. Evaluation of surface properties of reverse osmosis membranes on the initial biofouling stages under no filtration condition. J. Membr. Sci. 351 (1), 112–122.
Linden, K.G., Hull, N., Speight, V., 2019. Thinking outside the treatment plant: UV for water distribution system disinfection. Acc. Chem. Res. 52 (5), 1226–1233.
Ling, L., Tugaoen, H., Brame, J., Sinha, S., Li, C., Schoepf, J., Hristovski, K., Kim, J.-H., Shang, C., Westerhoff, P., 2017. Coupling light emitting diodes with photocatalyst-coated optical fibers improves quantum yield of pollutant oxidation. Environ. Sci. Technol. 51 (22), 13319–13326.
Liu, C., He, Q., Song, D., Jackson, J., Faria, A.F., Jiang, X., Li, X., Ma, J., Sun, Z., 2022. Electroless deposition of copper nanoparticles integrates polydopamine coating on reverse osmosis membranes for efficient biofouling mitigation. Water Res. 217, 118375.
Livak, K.J., Schmittgen, T.D., 2001. Analysis of relative gene expression data using real-time quantitative PCR and the 2− ΔΔCT method. Methods 25 (4), 402–408.
Loeb, S.K., Alvarez, P.J.J., Brame, J.A., Cates, E.L., Choi, W., Crittenden, J., Dionysiou, D. D., Li, Q.L., Li-Puma, G., Quan, X., Sedlak, D.L., Waite, T.D., Westerhoff, P., Kim, J. H., 2019. The technology horizon for photocatalytic water treatment: sunrise or sunset? Environ. Sci. Technol. 53 (6), 2937–2947.
Ma, L., Jackson, K.D., Landry, R.M., Parsek, M.R., Wozniak, D.J., 2006. Analysis of pseudomonas aeruginosa conditional psl variants reveals roles for the psl polysaccharide in adhesion and maintaining biofilm structure postattachment. J. Bacteriol. 188 (23), 8213–8221.
Mansouri, J., Harrisson, S., Chen, V., 2010. Strategies for controlling biofouling in membrane filtration systems: challenges and opportunities. J. Mater. Chem. 20 (22), 4567–4586.
Matin, A., Khan, Z., Zaidi, S.M.J., Boyce, M.C., 2011. Biofouling in reverse osmosis membranes for seawater desalination: phenomena and prevention. Desalination 281, 1–16.
Miller, D.J., Araújo, P.A., Correia, P.B., Ramsey, M.M., Kruithof, J.C., van Loosdrecht, M. C.M., Freeman, B.D., Paul, D.R., Whiteley, M., Vrouwenvelder, J.S., 2012. Short-term adhesion and long-term biofouling testing of polydopamine and poly(ethylene glycol) surface modifications of membranes and feed spacers for biofouling control. Water Res. 46 (12), 3737–3753.
Mo, Y., Tiraferri, A., Yip, N.Y., Adout, A., Huang, X., Elimelech, M., 2012. Improved antifouling properties of polyamide nanofiltration membranes by reducing the density of surface carboxyl groups. Environ. Sci. Technol. 46 (24), 13253–13261.
Molinari, R., Lavorato, C., Argurio, P., Szymański, K., Darowna, D., Mozia, S., 2019. Overview of photocatalytic membrane reactors in organic synthesis. Energy Storage Environ. Appl. Catal. 9 (3).
Mozia, S., 2010. Photocatalytic membrane reactors (PMRs) in water and wastewater treatment. A review. Sep. Purif. Technol. 73 (2), 71–91.
Muramoto, Y., Kimura, M., Nouda, S., 2014. Development and future of ultraviolet light-emitting diodes: UV-LED will replace the UV lamp. Semicond. Sci. Technol. 29 (8), 084004.
Nasrollahi, N., Ghalamchi, L., Vatanpour, V., Khataee, A., 2021. Photocatalytic-membrane technology: a critical review for membrane fouling mitigation. J. Ind. Eng. Chem. 93, 101–116.
Ni, L., Zhu, Y., Ma, J., Wang, Y., 2021. Novel strategy for membrane biofouling control in MBR with CdS/MIL-101 modified PVDF membrane by *in situ* visible light irradiation. Water Res. 188, 116554.
O'Neal Tugaoen, H., Garcia-Segura, S., Hristovski, K., Westerhoff, P., 2018. Compact light-emitting diode optical fiber immobilized TiO_2 reactor for photocatalytic water treatment. Sci. Total Environ. 613-614, 1331–1338.
Park, S.H., Ko, Y.S., Park, S.J., Lee, J.S., Cho, J., Baek, K.Y., Kim, I.T., Woo, K., Lee, J.H., 2016. Immobilization of silver nanoparticle-decorated silica particles on polyamide thin film composite membranes for antibacterial properties. J. Membr. Sci. 499, 80–91.

Pemmaraju, S.C., Padmapriya, K., Pruthi, P.A., Prasad, R., Pruthi, V., 2016. Impact of oxidative and osmotic stresses on Candida albicans biofilm formation. Biofouling 32 (8), 897–909.
Pezzoni, M., Pizarro, R.A., Costa, C.S., 2018. Exposure to low doses of UVA increases biofilm formation in pseudomonas aeruginosa. Biofouling 34 (6), 673–684.
Qiu, Z., Chen, J., Dai, R., Wang, Z., 2022. Modification of ultrafiltration membrane with antibacterial agent intercalated layered nanosheets: toward superior antibiofouling performance for water treatment. Water Res. 219, 118539.
Rana, D., Matsuura, T., 2010. Surface modifications for antifouling membranes. Chem. Rev. 110 (4), 2448–2471.
Reid, K., Dixon, M., Pelekani, C., Jarvis, K., Willis, M., Yu, Y., 2014. Biofouling control by hydrophilic surface modification of polypropylene feed spacers by plasma polymerisation. Desalination 335 (1), 108–118.
Rho, H., Cho, J., Westerhoff, P., Chon, K., 2020. Intrinsic pKa of nanofiltration membrane surfaces to assess fouling and cleaning behaviors induced by foulant–membrane electrostatic interactions. Environ. Sci. Technol. 54 (12), 7706–7714.
Rho, H., Chon, K., Cho, J., 2018. Surface charge characterization of nanofiltration membranes by potentiometric titrations and electrophoresis: functionality vs. zeta potential. Desalination 427, 19–26.
Rho, H., Chon, K., Cho, J., 2019. An autopsy study of a fouled reverse osmosis membrane used for ultrapure water production. Water 11 (6), 1116.
Rho, H., Im, S.J., Alrehaili, O., Lee, S., Jang, A., Perreault, F., Westerhoff, P., 2021. Facile surface modification of polyamide membranes using UV-photooxidation improves permeability and reduces natural organic matter fouling. Environ. Sci. Technol. 55 (10), 6984–6994.
Rice, D., Barrios, A.C., Xiao, Z., Bogler, A., Bar-Zeev, E., Perreault, F., 2018. Development of anti-biofouling feed spacers to improve performance of reverse osmosis modules. Water Res. 145, 599–607.
Rosenberg, E., DeLong, E., 2013. The Prokaryotes. Springer-Verlog, Berlin Heidelberg. Rosenberg EDE, Thompson F, Lory S, Stackebrandt E., editor.
Shannon, M.A., Bohn, P.W., Elimelech, M., Georgiadis, J.G., Mariñas, B.J., Mayes, A.M., 2009. Nanoscience and Technology. Co-Published with Macmillan Publishers Ltd, UK, pp. 337–346.
Sholtes, K.A., Lowe, K., Walters, G.W., Sobsey, M.D., Linden, K.G., Casanova, L.M., 2016. Comparison of ultraviolet light-emitting diodes and low-pressure mercury-arc lamps for disinfection of water. Environ. Technol. 37 (17), 2183–2188.
Song, H., Shao, J., He, Y., Liu, B., Zhong, X., 2012. Natural organic matter removal and flux decline with PEG–TiO_2-doped PVDF membranes by integration of ultrafiltration with photocatalysis. J. Membr. Sci. 405-406, 48–56.
Song, Y., Ling, L., Westerhoff, P., Shang, C., 2021. Evanescent waves modulate energy efficiency of photocatalysis within TiO_2 coated optical fibers illuminated using LEDs. Nat Commun. 12 (1), 4101.
Soule, T., Shipe, D., Lothamer, J., 2016. Extracellular polysaccharide production in a scytonemin-deficient mutant of nostoc punctiforme under UVA and oxidative stress. Curr. Microbiol. 73 (4), 455–462.
Tantra, R., Sikora, A., Hartmann, N.B., Sintes, J.R., Robinson, K.N., 2015. Comparison of the effects of different protocols on the particle size distribution of TiO_2 dispersions. Particuology 19, 35–44.
Torkzadeh, H., Zodrow, K.R., Bridges, W.C., Cates, E.L., 2021. Quantification and modeling of the response of surface biofilm growth to continuous low intensity UVC irradiation. Water Res. 193, 116895.
Wang, W., Huang, G., Yu, J.C., Wong, P.K., 2015. Advances in photocatalytic disinfection of bacteria: development of photocatalysts and mechanisms. J. Environ. Sci. 34, 232–247.
Wei, Y., Zhu, Y., Jiang, Y., 2019. Photocatalytic self-cleaning carbon nitride nanotube intercalated reduced graphene oxide membranes for enhanced water purification. Chem. Eng. J. 356, 915–925.
Winsor, G.L., Lam, D.K., Fleming, L., Lo, R., Whiteside, M.D., Yu, N.Y., Hancock, R.E., Brinkman, F.S., 2010. Pseudomonas genome database: improved comparative analysis and population genomics capability for pseudomonas genomes. Nucl. Acids Res. 39 (suppl_1), D596–D600.
Yang, Y., Alvarez, P.J.J., 2015. Sublethal concentrations of silver nanoparticles stimulate biofilm development. Environ. Sci. Technol. Lett. 2 (8), 221–226.
Zhao, Z., Lanzarini-Lopes, M., Westerhoff, E., Long, X., Rho, H., Bi, Y., Ling, L., Westerhoff, P., 2021. Evanescent wave interactions with nanoparticles on optical fiber modulate side emission of germicidal ultraviolet light. Environ. Sci.: Nano 8 (9), 2441–2452.